Atmos. Chem. Phys. Discuss., 9, 309–361, 2009
www.atmos-chem-phys-discuss.net/9/309/2009/

Atmospheric
Chemistry
and Physics
Discussions

Contributions from DMS and ship emissions to CCN observed over the summertime North Pacific

L. Phinney[1,*], W. R. Leaitch[2], U. Lohmann[3], N. C. Shantz[4], and D. R. Worsnop[5]

[1]Dalhousie University, Halifax, Nova Scotia, Canada
[2]Environment Canada, Toronto, Ontario, Canada
[3]Institute for Atmospheric and Climate Science, ETH Zurich, Switzerland
[4]University of Toronto, Toronto, Ontario, Canada
[5]Aerodyne Research Incorporated, Billerica, Massachusetts, USA
[*]now at: Meteorological Service of Canada, Dartmouth, Nova Scotia, Canada

Received: 18 September 2008 – Accepted: 7 October 2008 – Published: 6 January 2009

Correspondence to: L. Phinney (lisa.phinney@ec.gc.ca)

Published by Copernicus Publications on behalf of the European Geosciences Union.

Abstract

Measurements of cloud condensation nuclei (CCN) made over the remote North Pacific Ocean in July 2002 are analysed with concurrent measurements of aerosol number, mass and composition. Overall the CCN are controlled by the sulphate, including one case of particle nucleation and growth resulting from dimethyl sulphide oxidation that enhanced CCN concentrations. Hourly CCN concentrations are correlated with concentrations of sulphate plus methanesulphonic acid (MSA) over the entire study period (r^2=0.43 and 0.52 for supersaturations of 0.34 and 0.19%, respectively), and are not well correlated with other organics (r^2<0.2). One case study reveals elevated mass and number concentrations of ultrafine and fine organic particles due to regional ship emissions, during which organic mass concentrations (see Fig. 2). In Fig. 7c, the 80–90 nm particle concentrations are correlated with CCN values (r^2=0.39 and 0.46 for supersaturations of 0.19 and 0.34%, respectively). The evolution of the time series and mass distributions of organics, sulphate and MSA over this timeframe indicate that the regional distribution of small, diffuse ship-sourced organic particles act as condensation sites for sulphur species, resulting in a subsequent increase in number concentrations of CCN. Direct emissions of organic particles may exert a strong control on marine CCN concentrations once diffused into the marine atmosphere by acting as condensation sites for biogenic and anthropogenic sulphur species.

1 Introduction

The Canadian Surface Ocean – Lower Atmosphere Study (C-SOLAS) conducted the Subarctic Ecosystem Response to Iron Enrichment Study (SERIES) in the North Pacific Ocean in July, 2002 (Boyd et al., 2003). Goals of the study included characterizing the chemical and physical composition of the marine aerosol and investigating the processes that determine aerosol cloud condensation nuclei (CCN) concentrations in the remote marine environment. Sulphate and organics are dominant components of the fine particle marine aerosol (Quinn and Bates, 2005), yet their respective sources and their roles in the formation of CCN are still unclear. In particular, the role of organics in aerosol processes and cloud activation is poorly understood compared with that of sulphate. Lohmann and Leck (2005) identify the importance of surface-active submicron organic aerosols in explaining observed CCN concentrations in pristine Arctic clouds. The inclusion of only small amounts of internally-mixed soluble inorganics is found to dramatically increase the ability of organic aerosols to act as CCN, underscoring the importance of understanding the properties of an internally-mixed aerosol distribution (Lohmann et al., 2004). O'Dowd et al. (2004) suggest that organics, injected to the atmosphere through surface bubble activity, dominate the submicrometre aerosol number during marine bloom periods over the Atlantic Ocean, and the addition of the organic aerosol to sulphate+sea salt aerosol distributions can increase the cloud droplet number concentrations by 30–100%. The presence of organics in cloud droplets has been demonstrated by Russell et al., 2000.

Pirjola et al. (2000) show evidence for dimethyl sulphide (DMS)-derived particle nucleation in modelled marine boundary layer conditions, but question the possibility of observing nucleation events in the field due to insufficient sources of condensable material. Very few reports exist of new particle formation in the open ocean boundary layer (e.g. Clarke et al., 1998; Covert et al., 1992; Hoppel et al., 1990; Weber et al., 1998); the elevated concentrations of DMS in the SERIES sample region make it a promising location for investigating new particle formation and in general to look for evidence related to a DMS-CCN climate feedback mechanism. This feedback cycle, proposed by Shaw (1983) and Charlson et al. (1987), hypothesizes that nucleation, growth, and water uptake of sulphate and MSA derived from the oxidation of DMS leads to the modification of the reflectivities (Twomey, 1974) and lifetimes (Albrecht, 1989) of marine clouds. Here, the investigation is extended to the interaction of ship-sourced organics and the products of DMS oxidation in determining CCN concentrations in the marine environment.

Ship-going vessels have recently been identified as a major, weakly regulated global anthropogenic emissions source (i.e. MARPOL 73/78[1]; Corbett and Fischbeck, 1997). Ship emissions account for approximately 15% of both SO_2 and NO_x emissions globally (Corbett and Fischbeck, 1997), and the change in global radiative forcing due to the contribution of ship-sourced sulphate to CCN concentrations has been estimated to be $-0.11\,\mathrm{W\,m^{-2}}$, or 14% of total estimated indirect forcing from anthropogenic sulphate (Capaldo et al., 1999). The contribution of organic carbon to particulate matter emitted from an ocean-going vessel was estimated by Agrawal et al. (2008) to be 15% of the total PM mass. In the present study direct fumigation of the instruments from one of the three platforms involved in the study resulted in sharp increases in concentrations of small particulates, SO_2, and organic carbon, with little particulate sulphate (Phinney et al., 2006) as a result of the short time between emission and measurement of the plume, leaving little time for oxidation of SO_2 to sulphate. This points to the importance of organic carbon emissions from ocean-going ships, and moves us to investigate the impacts of these organics on the evolution of the aerosol and on CCN concentrations in the remote marine atmosphere. Russell et al (1999) note that during the Monterey Area Ship Tracks (MAST) experiment, "condensation of H_2SO_4 from gas-phase oxidation of SO_2 is primarily responsible for adding soluble sulphate mass to the newly emitted black and organic carbon particles". The authors emphasize the uncertainty in the relationship between organics and CCN, and conclude that the nature of the insoluble and slightly soluble carbon associated with ship emissions render it incapable of forming CCN under normal ambient supersaturations in the absence of sulphate.

In this paper, we examine the measurements of CCN, particle number distributions and chemical mass concentrations (principally sulphate, MSA and total organic) collected over the North Pacific Ocean to further our understanding of the relationship between aerosol chemical constituents and CCN in the marine environment.

---

[1] International Convention for the Prevention of Pollution from Ships, 1973, as modified by the Protocol of 1978 relating thereto: Annex VI – Regulations for the Prevention of Air Pollution from Ships, adopted 1997 and enforced as of 19 May 2005; www.imo.org.

2 Measurements

Atmospheric aerosol measurements were conducted from the Mexican Research Vessel El Puma as part of the SERIES study near ocean station Papa (50.0° N, 145.0° W) in the subarctic northeast Pacific (Fig. 1). Measurements were confined to a $1.5 \times 1.5^{\circ}$ grid and a transect made from Station Papa back to port in Sidney, British Columbia. Atmospheric measurements included size-resolved particle number concentrations and chemical composition, number concentrations of cloud condensation nuclei (CCN), trace gas mixing ratios, and meteorological variables. All times are reported as Pacific Daylight Savings Time (PDT; UTC-7). Local time in the sample area was approximately 1.5 h behind PDT, i.e. peak solar intensity in the sample area is observed at approximately 13:30 PDT.

Size-resolved aerosol number concentrations for particles with mobility diameters (D_m) between 8 and 290 nm were measured using a TSI Scanning Mobility Particle Sizer (SMPS; Model 3071 Electrostatic Classifier and a Model 3025 Ultrafine Condensation Particle Counter (UCPC)). For spherical particles with no internal voids, the mobility diameter is equal to the physical diameter (D_p). In this discussion, internal voids are assumed to be negligible, and the particles are considered to be spherical in the size range measured by the SMPS; thus the diameter measured by the SMPS is considered to be the physical diameter, D_p. Particle concentrations in each of 26 ranges of D_p were logged every 5 min. The accuracy of the particle concentration determined by the UCPC 3025 is ±10% up to 10^5 cm^{-3} (TSI, 2002).

An Aerodyne Quadrupole Aerosol Mass Spectrometer (Q-AMS) was used to obtain real-time quantitative measurements of the size and composition of non-refractory aerosol chemical species at 15-min resolution (Jayne et al., 2000). It does not allow for the measurement of refractory species, such as elemental carbon and sodium chloride, that evaporate slowly (t>a few seconds) at the temperature of the vaporizer. Non-refractory species that are internally-mixed with, or present on the surface of, refractory species (i.e. fine mode sea-salt-sulphate) are, however, detected by the

Q-AMS (Jimenez et al., 2003). The instrument provides information on individual particle sizes and ensemble mass loadings, with limited information on individual particle composition. The transmission of particles into the Q-AMS is nearly 100% in the range of 0.06 to 0.6 µm vacuum aerodynamic diameter (D_{va}), decreasing outside that range (Zhang et al., 2002; Liu et al., 2007). Detailed descriptions of the operation and calibration of the Q-AMS can be found elsewhere (i.e. Jayne et al., 2000; Zhang et al., 2002; Allan et al., 2003).

In the Q-AMS, the D_{va} of the particle is determined from its time-of-flight in the vacuum chamber. The D_{va} is related to the volume equivalent diameter (D_{ve}) according to:

$$D_{va}=\frac{\rho_p D_{ve}}{\rho_0 X_v}\ , \tag{1}$$

where ρ_p is the particle density (taking into account voids within the particle), ρ_0 is the reference density (unity), and X_v is the dynamic shape factor, defined as the ratio of the drag force on the particle to the drag force on its volume equivalent sphere, when both move at the same velocity with respect to the gas (DeCarlo et al., 2004). Here, since the aerosol contains a significant fraction (~60%) of sulphuric acid and the sampling was done at relatively high relative humidity, the particles are assumed to be spherical with no internal voids of zero density. Thus, D_{ve} is equal to the physical diameter, D_p, and the relationship of D_{va} to D_{ve} is simplified to:

$$D_{va}=\rho_p D_p\ . \tag{2}$$

A pleated capsule filter placed over the Q-AMS inlet for 45 min (i.e. 3 sample averages) resulted in the following detection limits: sulphate: 0.02 µg m^{-3}, MSA: 0.025 µg m^{-3}, nitrate: 0.015 µg m^{-3}, ammonium: 0.14 µg m^{-3}, organics: 0.20 µg m^{-3}. The mass concentrations of sulphate and MSA from the Q-AMS and those from size-segregated filter samples, collected with a static MOUDI, compared within 2 and 30%, respectively (Phinney et al., 2006). MSA was diagnosed for the first time using a Q-AMS in Phinney et al., 2006, and these data are used in the present work. Appendix A details

Title Page
Abstract | Introduction
Conclusions | References
Tables | Figures
◀| |▶
◀ ▶
Back | Close
Full Screen / Esc
Printer-friendly Version
Interactive Discussion

the experimental determination of the MSA fragmentation. Due to errors in the MSA fragmentation table at the time of analysis, the MSA mass concentrations presented in this paper are underestimated by less than 25%.

CCN observations were made using a University of Wyoming Model MA100 thermal gradient static cloud diffusion chamber (de Oliveira and Vali, 1995; Snider et al., 2006). Droplets grown in the chamber scatter light in proportion to their size, and the scattered intensity is converted to an analogue voltage. The CCN observations are reported here as deltaV, the difference between the voltage signal from the scattered light and the baseline voltage. The calibration factor for converting deltaV to number concentration varies with the size and composition of the particle as well as the supersaturation. This issue is discussed further in Shantz et al., 2008.

The SO_2 data were collected at 1-min resolution using a TECO Model 43C-TL SO_2 analyser. Zero air was periodically run through the instrument. The detection limit of 0.13 ppbv (0.37 $\mu g\,m^{-3}$) was determined from two standard deviations of the mean of the zero data. The baseline was interpolated in time from the 130 zero points. Calibrations were made using a diluted SO_2 NIST standard.

Measurements of SO_2, aerosol and CCN affected by direct emissions from the sampling platform (El Puma) during stationary periods, as well as one or two instances when the winds were from the stern at a greater speed than the ship's speed, have been removed. The occasional periods when exhaust from one of the other two sampling platforms (C.S.S. Tully, Canada, and Kaiyo Maru, Japan) directly affected the sampling have also been removed.

The atmospheric DMS data presented here were collected approximately every hour approximately 10 m above the sea surface (Phinney et al., 2006). Samples were analysed using a Hewlett Packard 5890 Gas Chromatograph equipped with a Sievers sulphur chemiluminescence detector (SCD Model 355). The analytical detection limit was 0.1 pptv.

The meteorological variables temperature, relative humidity, barometric pressure, relative wind speed, and relative wind direction were logged at 10-min intervals by the on-board meteorological instruments, located approximately 20 m above sea level. General meteorological conditions were overcast with several periods of fog, with clear sky periods exhibited on approximately six days. Winds were predominantly from the western quadrants at an average of 30 km h^{-1}. Information on other instrumentation used in this study can be found in Marshall et al. (2005), Phinney et al. (2006), and Shantz et al. (2008).

3 Results and analysis

3.1 Ambient aerosol time series

Time series' for data collected between 13–30 July 2002 are shown in Fig. 2; the mass concentrations of sulphate, total organics, and MSA measured by the Q-AMS in Fig. 2a, the number concentrations of particles in four ranges of physical diameter in Fig. 2b, and the observed deltaV for CCN activated at 0.19 and 0.34% supersaturations in Fig. 2c.

The mass concentration of sulphate varies from below detection limit (BDL) to 2.3 µg m^{-3}, MSA varies between BDL and 0.9 µg m^{-3}, and total organics range from BDL to 1.1 µg m^{-3}. Average mass concentrations are 0.78 µg m^{-3}, 0.16 µg m^{-3}, and 0.30 µg m^{-3}, respectively. The concentrations of MSA were an order of magnitude higher than concentrations observed over the North Pacific between Washington and Hawaii (Quinn et al., 1993), twice as high as those observed in the South Atlantic (Zorn et al., 2008) and also higher than that observed at Cape Grim, Tasmania (Andreae et al., 1999). The MSA concentrations reflect the elevated DMS concentrations in the region, which were four times greater than recent measurements over the North Pacific Ocean (Arinami and Tsunogai, 2004). The average sulphate mass concentration measured in this study is higher than the biogenic sulphate contribution to $PM_{2.5}$ of 0.3 µg m^{-3} measured on the Pacific Coast of Canada (Norman et al., 2006), and is also higher than the background marine concentration of 0.14 µg m^{-3} measured in the

Southern Ocean (Sievering et al., 2004). The mean organic concentration is lower than the levels measured on the west coast of Ireland (O'Dowd et al., 2004). The 18 July period, during which the highest organic mass concentrations were observed during this study (>1 µg m^{-3}), is examined in Sect. 4.

The number concentrations of particles with diameters less than 300 nm vary from 0 to 3500 cm^{-3} (Fig. 2b). The mean concentration of 500 cm^{-3} is at the upper end of typical marine boundary layer particle concentrations (e.g. Peng et al., 2002). A period of elevated concentrations of particles with diameters smaller than 58 nm is examined in Sect. 3.2.2.

The CCN observations show deltaV varying from 0.1 to 2.0 V for CCN active at 0.19% supersaturation ($CCN_{0.19\%}$) and from 0.2 to 7.3 V for CCN active at 0.34% supersaturation ($CCN_{0.34\%}$). The highest CCN concentrations were observed on 18 July, which coincides with the highest observed organic aerosol concentrations. Shantz et al. (2008) describe the CCN growth rates relative to the aerosol chemical and microphysical properties for the cases of 16, 18, and 27 July. In the present work, the factors controlling the CCN, and the evolution of the aerosol in two case studies, are examined.

3.2 Factors determining CCN

The supersaturations at which the CCN were measured (0.19 and 0.34%) are typical peak supersaturations for marine stratus and stratocumuli (e.g. Albrecht et al., 1989), the predominant cloud cover in this region during this study. Based on the Köhler equation and assuming the composition of sulphuric acid, the supersaturations of 0.19% and 0.34% activate particles with diameters larger than 86 nm and 58 nm, respectively. Sulphuric acid is used in the calculations because the majority of the aerosol mass (∼60%) is acidic sulphate (Phinney et al., 2006). Figure 3 shows the relationship between the CCN deltaV and the number concentration of aerosols with diameters larger than the critical radii at each supersaturation. The plots contain points for the entire time series (13–30 July). The r^2 values of 0.62 and 0.83 for 3a and b, respectively, indicate that most of the variance in the CCN is explained by the variance in the number concentrations of particles larger than the estimated theoretical activation diameter.

To give an idea of how these deltaV compare with particle numbers, Leaitch et al. (1999) determined a CCN number concentration calibration of 230 cm^{-3} per volt based on 150 nm monodisperse particles of $(NH_4)_2SO_4$ and NaCl exposed to 0.22% supersaturation. The inverse slope of Fig. 3a (the closest to 150 nm) is about 220, consistent with the above result.

The effects of sulphate, new particle formation, biogenic sulphate and organics on the CCN are investigated in the following sections.

3.2.1 Sulphate and CCN

In Fig. 4, deltaV for $CCN_{0.19\%}$ and $CCN_{0.34\%}$ are plotted against [MSA+SO_4] for the whole time series. Approximately 50% of the variations in the $CCN_{0.19\%}$ (r^2=0.53) and in the $CCN_{0.34\%}$ (r^2=0.48) are explained by variations in [MSA+SO_4]. The slope of the [MSA+SO_4]-$CCN_{0.34\%}$ trend line is three times higher than that of [MSA+SO_4]-$CCN_{0.19\%}$ since the total particle number concentration is higher at the smaller diameter corresponding to 0.34% supersaturation and also because the higher supersaturation will increase the growth rate of the particles and hence the relative amount of light scattered by the CCN. The lower values of r^2 compared with the correlations with number (Fig. 3) are primarily a consequence of the difference between measuring particle mass vs. number, i.e. most of the mass tends to be in large sizes.

3.2.2 Case study of new particle formation from DMS

On the afternoon of 14 July, number concentrations greater than 1000 cm^{-3} are observed for particles as small as 8 nm (Fig. 2b). Subsequent to the increase in the smallest measured particles, there was an increase in the number concentrations of particles with diameters of 30–60 nm through the morning of 15 July (Fig. 2b). The number concentrations of particles larger than 60 nm are relatively low during this time, and the sub-micron surface area available for condensational growth is lower by over

60% compared to the average value for this data series.

Figure 5a shows the change in particle size distribution (dN/d log D) with time for 14 July. The data exhibits a shape characteristic of particle nucleation and growth with peak number concentrations at diameters <10 nm preceding increases in larger particles over time (e.g. Kulmala et al., 2001; Buzorius et al., 2004). The concentrations of small particles begin to increase at about 14:00, and reach peak values at about 17:00. Prior to the increase in number concentrations, the particle surface area decreased by 55% (Fig. 5e), a factor favouring new particle formation in regions with lower levels of precursors (e.g. Clarke et al., 1998). A decrease in the relative humidity (RH) from 98% to 75% (Fig. 5a) occurs over the course of the increase in particle number concentrations between 12:00 and 15:00, likely the result of increasing temperature during the afternoon (Fig. 5b), and possibly due to mixing of dry air into the boundary layer. The reduced RH also will lower the ambient particle surface area.

The sulphate mass (Fig. 5b) is generally concentrated in particles with physical diameters between 150 and 400 nm (D_{va} between 250 and 700 nm), and is greater than 2.5 µg m^{-3} at times during this 42-h interval. Consistent with the reduction in the particle surface area, the concentration of sulphate in this size range decreases to below 0.4 µg m^{-3} between 12:00 and 18:00 on 14 July, prior to the increase in small particles shown in Fig. 5a. Sunny conditions, favourable for particle nucleation, were observed on 14 July in contrast to the more frequent and vast coverage by stratus and stratocumulus, and the second highest value of insolation for the time series was observed on 14 July at 15:00 PDT (Fig. 5d).

Corresponding to the rise in insolation on 14 July, the DMS concentration in the air decreases from approximately 6 µg m^{-3} (2 ppbv) at 10:30 to about 2 µg m^{-3} (0.7 ppbv) during the afternoon (Fig. 5c). An increase in the SO_2 concentration from approximately 0.2 ppbv to 0.35 ppbv is observed from 12:00 to 15:00 (Fig. 5d), coincident with the rise in MSA (Fig. 5c) and particle numbers (Fig. 5a), and prior to the increase in sulphate concentration at approximately 18:00 (Fig. 5b). The increase in MSA and SO_2 coincident with the decrease in DMS points to local-to-regional scale oxidation of DMS, while the rise in the sulphate concentration coincident with the growth of the particles (Fig. 5a and b) suggests condensation of oxidation products onto the nucleated aerosol particles.

The modelling work of Pirjola et al. (2000) indicates that in polar marine air masses binary H_2SO_4 nucleation can lead to particle concentrations on the order of $1000\,\mathrm{cm}^{-3}$, and ternary nucleation (H_2O-H_2SO_4-NH_3) can occur for marine boundary layer concentrations of sulphuric acid and ammonia concentrations on the order of $0.002\,\mu\mathrm{g\,m}^{-3}$ and 5 pptv, respectively. The authors suggest that ternary nucleation will result in enhancements in nanoparticles only for DMS concentrations greater than approximately of 0.4 ppbv. In our sample region DMS concentrations reached nearly 8 ppbv, with a mean concentration of about 2 ppbv. While ammonia was not measured during this study, Quinn et al. (1992) report concentrations of gas-phase ammonia of approximately 20 pptv over the north east Pacific Ocean, sufficient to initiate ternary nucleation based on the model calculations of Pirjola et al. (2000). Thus, the sampled conditions were favourable and the results consistent with the possibility of ternary or binary particle nucleation.

During the 14 July nucleation event, the wind speed was 25–$30\,\mathrm{km\,h}^{-1}$ and increases in small particle concentrations are seen approximately 6 h after DMS concentrations begin to decrease with the increase in solar irradiation at 09:00. The average winds were from the west, and for a 6-h lag time for nucleation the source region would have had to extend at least 200 km to the west.

Figure 5e indicates that between 12:00 and 18:00 the deltaV for smaller CCN ($\mathrm{CCN}_{0.34\%}$) increases, corresponding to the increases in particle concentrations. The deltaV for larger CCN ($\mathrm{CCN}_{0.19\%}$) does not change significantly during this time, consistent with the sulphate distribution which does not start to show significant mass until after 18:00. Between 18 July 18:00 and 19 July 01:00, the concentrations of the smaller CCN decrease as the mass concentrations of sulphate and MSA, as well as the particle surface area, all increase. A closer look at the sulphate mass distribution reveals that the mode diameter decreased as the distribution broadened throughout the overnight period (Fig. 5b). This occurs because as mass condenses onto the entire distribution, the more numerous particles at the lower end of the distribution grow into the Q-AMS detection range (>50 nm) while the particles on the upper end grow out of the Q-AMS detection range >1000 nm).

The evidence presented above suggests particle nucleation from biogenic sulphate precursors was observed during our study. Concentrations of CCN increased during this event, then decreased as the particle distribution broadened. The following section examines the role of biogenic sulphate on CCN concentrations.

3.2.3 Biogenic sulphate and CCN

Higher mass concentrations of MSA are a marker for DMS oxidation and biogenic sulphate. To investigate the general relationship of biogenic sulphate and CCN in this study, properties of the aerosol during times associated with peak MSA concentrations greater than 0.45 $\mu g\, m^{-3}$ (the 98th percentile value) are compared with those during times when MSA concentrations are lower than 0.45 $\mu g\, m^{-3}$. DeltaV for $CCN_{0.19\%}$ and $CCN_{0.34\%}$ increase by 30% during times associated higher MSA concentrations (20 July and 27 July) over those with lower MSA concentrations (Table 1). The slope of the sulphate-$CCN_{0.19\%}$ relationship increases by 45% when MSA concentrations are higher (the slope of the sulphate-$CCN_{0.34\%}$ relationship showed no change). Possible explanations for the increase in CCN and slope may include a smaller CCN effective diameter or greater aerosol activation when MSA is present. Figure 6a and b show the normalized number and volume distributions, respectively, of particles measured during times of high and low MSA concentration. The number distribution indicates a relative increase in numbers of particles >58 nm (theoretical activation diameter for $CCN_{0.34\%}$) and >86 nm (theoretical activation diameter for $CCN_{0.19\%}$) when MSA concentrations are high, and shows that the distribution of particles large enough to act as CCN is not shifted towards smaller sizes. This indicates that the increases in CCN and slope are due to an increase in the number concentrations of CCN above the critical radius rather than a change in the CCN effective radius. Figure 6b indicates that, though the CCN numbers increase, changes in the volume (proportional to mass) distribution are not apparent for particles in the activation range. This comparison of number and volume distributions at lower and higher MSA concentrations suggests that the impact of DMS oxidation on CCN in this instance is to increase the number concentrations of CCN active at supersaturations representative of marine stratiform clouds.

3.2.4 The role of organics

Figure 7a shows the correlation between the mass concentration of [MSA+SO_4] and particles in the 200–300 nm physical diameter size range for 13–30 July. Of the particle size ranges shown in Fig. 2b, this size range is best correlated with [MSA+SO_4]; much of the variation in particles of this size can be explained by variations in [MSA+SO_4]. In the case of the 80–90 nm particles vs. [MSA+SO_4] (Fig. 7b), two distinct trends are apparent. The upper trend is identified by episodes of higher number concentrations of 80–90 nm particles (up to 450 cm^{-3}), and the leading and trailing tails of these episodes. The majority of these points occur during a 20-h period on 18 July, a day with higher aerosol mass and number concentrations, including the highest measured organic mass concentrations (Fig. 2). In Fig. 7c, the 80–90 nm particle concentrations are plotted versus the organic mass concentrations for this 20-h period. The coefficient of variation for the fit of the 80–90 nm particles with organic mass (Fig. 7c) is lower than with [MSA+SO_4] (upper curve of Fig. 7b), but the slope is over twice as high. This suggests that 80–90 nm particles are considerably more sensitive to increases in organic mass than in sulphur mass for this particular situation. Since the plots refer to the same size range of particle concentrations, this result suggests that the organics and sulphate are not homogeneously mixed. It is hypothesized that the increase in organic mass is directly related to increases in particles, whereas most of the sulphur mass condenses onto pre-existing particles, increasing mass concentrations but leaving numbers of particles unchanged. This hypothesis is investigated here.

Surface back trajectories were generally from the west during the study (13–30 July), but the surface and upper air analyses for 18 July show a quasi-stationary low, during which time the winds were light and the skies were clear (Fig. 8). Back trajectories show no contact with the continent as far back as five days (Fig. 8a). The concentrations of organics in the aerosol reach nearly 1 µg m^{-3}, the highest concentrations observed during the study, and were sustained above 0.5 µg m^{-3} for nearly 24 h (Fig. 2a).

The mass spectrum of organic fragments from the Q-AMS averaged for the entire sample period (13–30 July), excluding 18 July and direct fumigation by ship exhaust, is shown in Fig. 9a, plotted as intensities relative to the highest peak. The highest contribution is from *m/z* 44, a signature of oxygenated organic compounds such as di- and poly-carboxylic acids, whose fragments contain CO_2^+ which dissociates from the organic molecule when hitting the vaporizer (Allan et al., 2004). The mass spectrum has contributions from the series (*m/z* 27, 41, 55, 69, ...), indicative of unsaturated hydrocarbons, whose masses are relatively more abundant than the series (*m/z* 29, 43, 57, 71, ...) which is representative of saturated hydrocarbons (Canagaratna et al., 2004). The mass fragment at *m/z* 43 can have contributions both from saturated hydrocarbons and oxidized organic species such as aldehydes or ketones. The peaks at *m/z* 77 and 91 are indicative of aromatic hydrocarbons (Canagaratna et al., 2004). By comparison the relative mass spectrum during a period of fumigation from the exhaust of our platform, El Puma, indicates a composition almost exclusively of hydrocarbons (alkanes, *m/z* 29, 45, 57, 71, 85, ...; *m/z* 27, 41, 55, 69, 83, ..., and *m/z* 67, 81, 95, ...) (Fig. 9b).

The average spectrum for 18 July (Fig. 9c) shows a relative reduction in the intensity of *m/z* 44 and relative enhancements in *m/z* 43 and 57 compared with Fig. 9a. The increased relative abundance of the hydrocarbon mass fragments (e.g. *m/z* 67, 69, 71, 81, 83, 85, 95, 97, 109, 111) indicates evidence of a significant influence from a combustion source. The ratio of *m/z* 44 to the total organics concentration is both lower and more stable on 18 July than for other times (Fig. 9d), indicating a relatively non-oxygenated aerosol across this period compared with the study average. However, the oxygenated carbon content was not as low as that of direct ship exhaust, thus it gives the appearance of either slightly aged diesel emissions or diesel emissions mixed with a more oxygenated organic aerosol of other origin. Based on the atmospheric circulation and the mass spectra, it is conjectured that emissions from ships crossing the region slowly circulated, diffused, and eventually impacted our measurements.

Figure 10 shows an expanded view of Fig. 2, covering only 18 July. Vertical bars divide the event into six time periods (Period I 00:00–03:45; Period II 03:45–06:00; Period III 06:00–07:30; Period IV 09:00–12:30; Period V 12:30–17:30; and Period VI 18:00–23:30). These six intervals are chosen based on changes in the CCN and the relative concentrations of organic and sulphate masses. Period I is characterized by lower particle number concentrations and CCN scattering, and the average organic and sulphate mass concentrations are 0.33 µg m^{-3} and 1.04 µg m^{-3} respectively. In Period II, the number concentrations of particles with diameters less than 86 nm increase from 700 to nearly 2000 cm^{-3}, and the CCN active at 0.34% supersaturation increase. The mean organic and sulphate mass concentrations are 0.30 µg m^{-3} and 0.96 µg m^{-3} respectively, very close to those of Period I. However, there is a broadening in both sulphate and the organic mass distributions towards smaller sizes from Period I to II (Fig. 11), consistent with the increase in smaller particles and CCN. During Period III, there is a brief period of increased concentrations of particles smaller than 58 nm, coincident with a rise in organics (Fig. 10), while sulphate and MSA concentrations remain steady or decrease slightly. The mass distributions during this time show a distinct shoulder mode developing in MSA and sulphate at D_{va}=150 nm, with a corresponding developing mode in organics (Fig. 11). Concentrations of organics increase slightly to 0.6 µg m^{-3}, while sulphate has decreased to 0.87 µg m^{-3}. Period IV is characterized by increases in the organic and sulphate mass concentrations. During this time, particles with diameters less than 200 nm increase while particles smaller than 58 nm decrease (Fig. 10), and the developing small mode at 150 nm is more prominent in sulphate, MSA, and especially organics (Fig. 11). Period V is characterized by an increase in particles with diameters greater than 86 nm, and an increase in CCN$_{0.34\%}$. The organic is relatively constant throughout the period, but it is three times higher in Period V (0.92 µg m^{-3}) relative to Periods I and II, and sulphate is also higher in Period V (1.36 µg m^{-3}). The mass distribution in Period V shows the small mode that had developed at 150 nm has grown to a modal diameter of 180 nm as the mass concentration increases. Finally, in Period VI the concentration of organics decreases to 0.68 µg m^{-3} while the sulphate concentration increases and then decreases, and $CCN_{0.19\%}$ increase. The size spectrum of the sulphate (Fig. 11) shows it is returning to a monomodal distribution, but is still skewed towards smaller sizes compared with Period I.

The progression from Periods I through VI indicates an evolution of the aerosol from an internal mixture of organic and sulphate in Period I to a more external organic-sulphate mixture in Period's II through IV with more organic mass at smaller sizes, and finally in Periods V and VI to a more internal mix of organics and sulphate with fewer smaller particles and less mass at smaller sizes, and more larger CCN. It is evident that during periods III and IV there are different mixes of organics and sulphate. By period V, sulphate and organics have similar distributions, except below 100 nm D_{va}. In the presence of biogenic sulphur the smaller organic particles from ship emissions act as condensation sites for the sulphate and MSA, eventually returning the aerosol to an internal mix of organics, MSA and sulphate. These observations support the above hypothesis, and the increase in particle number concentrations shown in Fig. 7c, which occurs largely during this 18 July time period, is attributed to the presence of the organics. The organics provide a distribution of small, numerous particles to act as condensation sites for the sulphate and MSA, subsequently activating as CCN at supersaturations typical of marine stratus clouds.

3.2.5 Organics and CCN

During the evolution of the aerosol on 18 July, the condensation of sulphate and MSA onto the smaller organic particles affects the level of CCN activity. Figure 10 showed an increase first in smaller CCN ($CCN_{0.34\%}$) as small organics increased, followed by an increase in larger CCN ($CCN_{0.19\%}$) as sulphate and MSA concentrations increased at larger sizes. In Fig. 12a and b, the correlations of organics and of [MSA+SO_4] each with CCN are shown for the entire sample period excluding 18 July. In Fig. 12c and d the same regressions are shown for the 18 July time period only. The correlation of CCN with organics throughout the entire study is weak (Fig. 12a), whereas the correlation of CCN with [MSA+SO_4] is much higher (Fig. 12b), indicating that the sulphur species exert some control over the CCN. For the time period of 18 July, however, a different pattern emerges. In this case, the CCN correlate better with organics (Fig. 12c) than with [MSA+SO_4] (Fig. 12d), and those correlations with organics are significantly higher than those for the whole sample period. Over the entire study period the CCN are controlled by the MSA and sulphate, but on 18 July when the concentrations of organics increase due to suspected regional ship emissions, these particles exert more control over the CCN than do the sulphur species. The slope of the regression for $CCN_{0.34\%}$ increases by about 50% during the 18 July time period compared with the rest of the sample period, for both sulphate and organics. Thus, for a given mass concentration there is 50% more scattering by CCN on 18 July than for the rest of the sample period. This may indicate larger CCN or higher CCN concentrations, or some combination of the two. This difference in slope is not evident for $CCN_{0.19\%}$, suggesting that these CCN are more associated with larger particles where the sulphate accumulates through condensation.

It is interesting that the correlation of sulphate with organics during the 18 July time period is relatively weak (Fig. 13a). A close look at Fig. 10 reveals that the sulphate and organics exhibit a similar shape but shifted in time, with sulphate rising after the organics. The correlation between [MSA+SO_4] and organics is highest (r^2=0.57) when the sulphate and MSA time series are shifted back by 2.5 h (Fig. 13b). This time delay in MSA and sulphate concentrations requires further investigation, but lends support to the theory that sulphate and MSA condense onto the organics over time, resulting in a delayed increase in their mass concentrations relative to the increase in organics.

The influence of organics on CCN for higher mass fractions of organic in the particles has been observed for anthropogenic aerosols (Chang et al., 2007; Wang et al., 2008), suggesting that the organic material can significantly impact the water uptake. However, in the 18 July case water uptake does not appear to be the main role of the organic mass (Shantz et al., 2008). Rather, the higher slopes of CCN versus [MSA+SO_4] for this time period reflect the sulphate and MSA distributing over a larger number of particles (principally primary organic emissions), yielding more CCN for a given value of [MSA+SO_4].

4 Summary and conclusions

Seasonal relationships have been found between DMS, MSA, and cloud condensation nuclei (CCN) in the marine environment (Ayers and Gras, 1991; Ayers et al., 1991; Andreae et al., 1995), and correlations among sulphate, MSA, and SO_2 on a shorter temporal scale are reported in Huebert et al. (1996). In Phinney et al., 2006, DMS and MSA showed anti-correlated behaviour, while anti-correlations in DMS and SO_2 are reported elsewhere (i.e. Davis et al., 1999). The variations in these relationships are in part owing to the timescale of sampling. Similarly, in contrast to the findings of Hegg et al. (1991), no correlation between DMS and CCN was found during this study. This is not surprising considering that the timescale for oxidation of DMS is on the order of hours to one day and that our measurements are at 15-min to 1-h resolution. High wind speeds will complicate these relationships over the relatively short timescales and small geographical distribution of our measurements.

With one exception, the baseline CCN concentrations over 18 days were maintained without obvious nucleation events, and several periods of increased CCN were observed without accompanying nucleation events. The one exception was from 14 July. On that day, increased nanoparticle concentrations corresponded to a decrease in gaseous SO_2 concentrations that followed a decreased in DMS concentrations. About 6 h later, an increase in the CCN was observed. The increase in the CCN was consistent with the growth and evolution of particle size, linking the CCN increase back to the oxidation of DMS. The timeframe for nucleation and growth of particles to detectable sizes implies that the DMS source region was 200–400 km upwind (to the west) of the sample region.

The most significant results of this paper relate to the interaction between organics and sulphate in the marine environment. Our findings suggest that naturally-derived aerosols are not solely responsible for a DMS-sulphate-CCN connection as proposed by Shaw (1983) and Charlson et al. (1987), nor do biogenic marine organics play a large role in CCN in this environment as in O'Dowd et al., 2004. In general, the CCN observed in this study were significantly correlated with MSA and sulphate, and were not correlated with organic mass concentrations. However, in one case (18 July), an increase in particulate organic mass associated with regional ship emissions increased the number concentrations of particles with diameters less than 90 nm, and MSA and sulphate mass concentrations increased 2–3 h later. The organics during this time were correlated with CCN scattering voltages, and the evolution of the mass distributions of organics, sulphate and MSA indicate the sulphur species condensed onto the smaller organic particles. Over several hours the aerosol evolved to become more internally-mixed with most particles >90 nm, and the CCN signal increased. Thus, while the condensation of sulphate and MSA is essential for the activation of the aerosols as CCN, regionally diffused primary emissions of organic particles over the ocean can have a dominant influence on the number concentrations of particles active at supersaturations typical of marine stratocumuli.

Finally, O'Dowd et al. (2004) suggested that the concentrations of marine biogenic organics in the atmosphere over the Atlantic Ocean are especially high during plankton bloom periods, and discuss implications for the marine biota-aerosol-cloud-climate feedback mechanism. Here we find little support for a role of these particles as CCN, as evidenced by the weak correlation of organics with CCN over the entire sample period. Rather, our findings point to sulphur compounds and ship-sourced organics together having the greatest impact on CCN over the NE Pacific.

Appendix A

Determination of MSA mass concentrations with the Q-AMS

Laboratory experiments to determine the fragmentation pattern of methanesulphonic Acid (MSA) were conducted independently at Environment Canada, Downsview, ON, and Aerodyne Research Incorporated, Billerica, MA, May 2003. Prior to these laboratory experiments, the Q-AMS signal due to MSA fragments was attributed to sulphate, ammonium and organics. These laboratory experiments were designed to determine what portion of certain sulphate, ammonium and organic fragments should be attributed to MSA.

A1 Theory

Methanesulphonic acid (MSA) has the chemical formula CH_3SO_3H, and molecular weight 96.11 amu/molecule. The chemical structure of MSA is

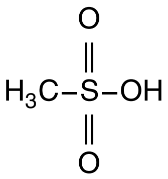

$$H_3C-\overset{\overset{\displaystyle O}{\|}}{\underset{\underset{\displaystyle O}{\|}}{S}}-OH$$

where the methyl group and hydroxyl group are single-bonded to the S atom and the oxygen molecules are double-bonded to the S atom. The MSA molecule, upon flash vaporization and ionization in the vacuum vaporization chamber of the AMS, is expected to fragment at the single bonds C–S and S–OH, yielding fragments at *m/z* 15 (CH_3^+) and at *m/z* 17 (OH^+). As well, signals at *m/z* 14 (CH_2^+), 16 (CH_4^+), 31 (CH_3O^+), 48 (SO^+), 64 (SO_2^+), 65 (HSO_2^+), 78 ($CH_2SO_2^+$), 79 ($CH_3SO_2^+$), (80 (SO_3^+), 81 (HSO_3^+), and 96 (MSA^+) may be expected. The NIST spectrum for MSA consists of highest peaks at *m/z* 96, 79, 81, 78, 31, 65, and 48, in decending order of intensity (NIST, 2005).

A2 Experimental setup

The Q-AMS was connected downflow of an atomizer generating a polydisperse aerosol population from a dilute solution. In between the atomizer and the Q-AMS was placed a silica cartridge for drying the particles leaving the atomizer, and a TSI Differential Mobility Analyser (DMA; Model 3071 Electrostatic Classifier and a Model 3025 Ultrafine Condensation Particle Counter), which selects a monodisperse aerosol population from the polydisperse aerosol generated by the atomizer.

A3 Procedure

Solutions of pure ammonium sulphate ($(NH_4)_2SO_4$), pure MSA, and a mixture of MSA and $(NH_4)_2SO_4$ were diluted to a concentration of ~0.01 M using de-ionized water (DIW).

The Q-AMS was calibrated to ensure optimal performance: the electron multiplier was calibrated for the gain, and then a mass calibration was done to determine the ionization efficiency of nitrate, a standard calibration procedure for the Q-AMS.

Particles were generated by atomizing the solutions of MSA and ammonium sulphate, and the particles were measured by the Q-AMS in mass spectrum mode to obtain a relative mass spectrum from which to create a fragmentation pattern for MSA, and then in time-of-flight mode to determine the ionization efficiency of MSA. Table A1 describes the solution mixtures and size distribution characteristics of the trials.

A3.1 Pure $(NH_4)_2SO_4$ solution

A 0.01 M solution of $(NH_4)_2SO_4$ was placed in the atomizer bottle and sampled by the AMS. A mass spectrum was obtained, shown in Fig. A1. Peaks attributed to NH_4^+

fragmentation are observed at m/z 15, 16, and 17, and peaks attributed to SO_4^{2+} fragmentation are observed at m/z 18, 32, 48, 64, 80, 81, and 98. The mass fragment at m/z 18 is due to remnant H_2O present on the ammonium sulphate particles, and relative humidity within the instrument.

A3.2 MSA+$(NH_4)_2SO_4$ solution

The atomizer bottle was rinsed with DIW and filled with a 0.01 M solution of MSA and $(NH_4)_2SO_4$. The mass spectrum obtained by the AMS is shown in Fig. A2. Peaks attributed to ammonium are observed at m/z 15, 16 and 17, and peaks attributed to sulphate are observed at m/z 32, 48, 64, 65, 80, 81, and 98. Peaks attributed to organics in this batch file are observed at m/z 12,13, 15, 29, 44, 45, 64, 65, 78, 79, and 96. Because we have not included organics in our atomized solution, these peaks, along with a portion of those diagnosed here as sulphate, are likely due to the fragmentation of MSA.

A3.3 Pure MSA solution

A pure 0.001 M MSA solution was atomized and 300 nm particles were selected with the DMA. The mass spectra are shown in Fig. A3. All of the MSA is currently attributed to sulphate and organics; peaks are observed at m/z 14, 15, 16, 29, 31, 48, 64, 65, 78, 79, 81, and 96.

Figure A4 shows the mass spectrum when the DMA was adjusted to 0 V, meaning no particles should enter the Q-AMS.

A4 Results

Figures A1 through A3 show the mass spectrum obtain through each of the solution trials. These plots were analysed with the previous version of the fragmentation file, which did not include MSA fragmentation (Allan et al., 2004), thus all MSA is currently attributed to sulphate and organic fragmentation. After examination of these plots, the fragment *m/z* 79 was used as the basis for the identification of MSA because there is no contribution to this fragment from ammonium sulphate or sulphuric acid, but a strong signal is detected when measuring MSA. Fragments 15, 29, 31, 45, 65, and 78 were also identified through the fragmentation pattern as having contributions from MSA, and were calculated in relation to the signal at *m/z* 79. In this way, a fragmentation table for MSA was developed and incorporated into the analysis of the SERIES data, enabling the identification of MSA.

The fragmentation table resulting from this procedure is given in Table A2. Fragments whose determinations have been modified from the previous version of the fragmentation table (Allan et al., 2004), as well as the new MSA fragments, have been noted in boldface. Figure A5 shows the resultant mass spectrum of MSA after analysing the data displayed in Fig. A3 with the new fragmentation table. MSA is shown in purple, and its identification results in a reduction in the previously estimated concentrations of sulphate and organics, since all the mass that is now attributed to MSA was attributed to these species under the previous fragmentation table. Due to small errors in estimating the contributions of fragments to the MSA mass calculation, the MSA spectrum still shows contributions from ammonium fragments and from sulphate fragments. The resulting underestimation in the MSA mass calculation is estimated to be less than 25%. Because the average mass concentration of sulphate in the SERIES experiment was nearly five times as high as the MSA mass concentration, the resulting error in the sulphate mass measured by the Q-AMS is much smaller (approximately 5%).

This new fragmentation table has been used to analyse all the Q-AMS data presented in this paper and in Phinney et al. (2006). In the 2006 paper, the use of this fragmentation table was shown to result in measurements of MSA and sulphate that were in good agreement with measurements obtained through filter analysis and from estimation based on aerosol physical properties; however the 25% underestimation is evident in the comparison between Q-AMS and MOUDI measurements of MSA mass concentration. Further independent experiments conducted at Aerodyne Research, Incorporated obtained a mass spectrum of MSA that showed excellent agreement with our laboratory results.

Acknowledgements. The authors thank J. Marshall, S. Bacic, A. Gaudenzi, J. Jayne, H. Boudries, D. Toom-Sauntry, D. Halpin, S. Sharma and the captain, crew and fellow scientists of El Puma for help with data collection and analysis. The DMS data presented in this paper was collected by Moire Wadleigh and Carolyn Burridge. L. Phinney extends appreciation to the Meteorological Service of Canada – Atlantic. This work was funded by the joint NSERC/CFCAS project SOLAS and by Environment Canada; N. Shantz was supported in part by an NSERC PGS-B research scholarship.

References

Agrawal, H., Malloy, Q. G. J., Welch, W. A., Miller, J. W., and Cocker III, D. R.: In-use gaseous and particulate matter emissions from a modern ocean going container vessel, Atmos. Environ., 42, 5504–5510, 2008.

Albrecht, B. A.: Aerosols, cloud microphysics, and fractional cloudiness, Science, 245, 1227–1230, 1989.

Allan, J. D., Jimenez, J. L., Williams, P. I., Alfarra, M. R., Bower, K. N., Jayne, J. T., Coe, H., and Worsnop, D. R.: Quantitative sampling using an Aerodyne aerosol mass spectrometer 1. Techniques of data interpretation and error analysis, J. Geophys. Res., 108, 4090–4100, 2003.

Allan, J. D., Delia, A. E., Coe, H., Bower, K. N., Alfarra, M. R., Jimenez, J. L., Middlebrook, A. M., Drewnick, F., Onasch, T. B., Canagaratna, M. R., Jayne, J. T., and Worsnop, D. R.: A generalised method for the extraction of chemically resolved mass spectra from Aerodyne aerosol mass spectrometer data, J. Aerosol Sci., 35, 909–922, 2004.

Andreae, M. O., Elbert, W., Cai, Y., Andreae, T. W., and Gras, J.: Non-sea salt sulfate, methanesulfonate, and nitrate aerosol concentrations and size distributions at Cape Grim, Tasmania, J. Geophys. Res.,104, 21695–21706, 1999.

Andreae, M. O., Elbert, W., and de Mora, S. J.: Biogenic sulfur emissions and aerosols over the tropical South Atlantic, 3. Atmospheric dimethylsulfide, aerosols and cloud condensation nuclei, J. Geophys. Res., 100, 11335–11356, 1995.

Arinami, K. and Tsunogai, S.: Seasonal and regional comparison of oceanic and atmospheric dimethyl sulphide in the northern North Pacific: dilution effects on its concentration during the winter, J. Geophys. Res., 109, 4288, D12303.1–D12303.15, 2004.

Ayers, G. P., Ivey, J. P., and Gillett, R. W.: Coherence between seasonal cycles of dimethyl sulphide, methanesulphonate, and sulphate in marine air, Lett. Nature, 349, 404–406, 1991.

Ayers, G. P. and Gras, J. L.: Seasonal relationship between cloud condensation nuclei and aerosol methanesulphonate in marine air, Lett. Nature, 353, 834–835, 1991.

Boyd, P. W., Law, C. S., Wong, C. S., Nojiri, Y., Tsuda, A., Levasseur, M., Takeda, S., Rivkin, R., Harrison, P. J., Strzepek, R., Gower, J., McKay, R. M., Abraham, E., Arychuk, M., Barwell-Clarke, J., Crawford, W., Hale, M., Harada, K., Johnson, K., Kiyosawa, H., Kudo, I., Marchetti, A., Miller, W., Needoba, J., Nishioka, J., Ogawa, H., Page, J., Robert, M., Saito, H., Sastri, A., Sherry, N., Soutar, T., Sutherland, N., Taira, Y., Whitney, F., Wong, S.-K. E., and Yoshimura, T.: The decline and fate of an iron-induced subarctic phytoplankton bloom, Nature, 428, 549–553, 2003.

Broekhuizen, K., Kumar, P. P., and Abbatt, J. P. D.: Partially soluble organics as cloud condensation nuclei: Role of trace soluble and surface active species. Geophys. Res. Lett., 31, L01107, doi:10.1029/2003GL018203, 2004.

Buzorius, G., McNaughtonm, C. S., Clarke, A. D., Covert, D. S., Blomquist, B., Nielsen, K., and Brechtel, F. J.: Secondary aerosol formation in continental outflow conditions during ACE-Asia, J. Geophys. Res., 109, 4749, doi:10.1029/2004JD004749, 2004.

Canagaratna, M. R., Jayne, J. T., Ghertner, D. A., Herndon, S., Shi, Q., Jimenez, J. L., Silva, P. J., Williams, P., Lanni, T., Drewnick, F., Demerjian, K. L., Kolb, C. E., and Worsnop, D. R.: Chase Studies of Particulate Emissions from in-use New York City vehicles, Aerosol. Sci. Tech., 38, 555–573, 2004.

Capaldo, K., Corbett, J. J., Kasibhatla, P., Fischbeck, P., and Pandis, S. N.: Effects of ship emissions on sulphur cycling and radiative climate forcing over the ocean, Nature, 400, 743–746, doi:10.1038/23438, 1999.

Chang, R. Y.-W., Liu, P. S. K., Leaitch, W. R., and Abbatt, J. P. D.: Comparison between measured and predicted CCN concentrations at Egbert, Ontario: Focus on the organic aerosol fraction, Atmos. Environ., 41, 8172–8182, 2007.

Charlson, R. J., Lovelock, J. E., Andreae, M. O., and Warren, S. G.: Oceanic phytoplankton, atmospheric sulphur, cloud albedo, and climate, Nature, 326, 655–661, 1987.

Clarke, A. D., Davis, D., Kapustin, V. N., Eisele, F., Chen, G., Paluch, I., Lenschow, D., Bandy, A. R., Thorton, D., Moore, K., Mauldin, L., Tanner, D., Litchy, M., Carroll, M. A., Collins, J., and Albercook, G.: Particle nucleation in the tropical boundary layer and its coupling to marine sulfur sources, Science, 282, 89–92, 1998.

Corbett, J. J. and Fischbeck, P. S.: Emissions from ships, Science 278, 823–824, 1997.

Covert, D. S., Kapustin, V. N., Quinn, P. K., and Bates, T. S.: New particle formation in the marine boundary layer, J. Geophys. Res., 97, 20581–20589, 1992.

Davis, D., Chen, G., Bandy, A., Thornton, D., Eisele, F., Mauldin, L., Tanner, D., Lenschow, D., Fuelberg, H., Huebert, B., Heath, J., Clarke, A., Blake, D.: Dimethyl sulphide oxidation in the equatorial Pacific: Comparison of model simulations with field observations for DMS, SO_2, H_2SO_4(g), MSA(g), MS and NSS, J. Geophys. Res., 104, 5765–5784, 1999.

De Bruyn, W. J., Dahl, E., and Saltzman, E. S.: DMS and SO2 Measurements in the tropical marine boundary layer, J. Atmos. Chem., 53, doi:10.1007/s10874-005-9000-z, 2006.

DeCarlo, P., Slowik, J. G., Worsnop, D. R., Davidovits, P., and Jimenez, J. L.: Particle morphology and density characterization by combined mobility and aerodynamic diameter measurements. Part 1: Theory, Aerosol Sci. Tech. 38, 1185–1205, 2004.

de Oliveira, J. C. P. and Vali, G.: Calibration of a photoelectric cloud condensation nucleus counter, Atmos. Res., 38, 237–248, 1995.

Hegg, D. A., Radke, L. R., and Hobbs, P. V.: Measurements of Aitken nuclei and cloud condensation nuclei in the marine atmosphere and their relation to the DMS-cloud-climate hypothesis, J. Geophys. Res., 96, 18727–18773, 1991.

Hoppel. W. A., Fitzgerald, J. W., Frick, G. M., Larson, R. E., and Mack, E. J.: Aerosol size distributions and optical properties found in the marine boundary layer over the Atlantic Ocean, J. Geophys. Res., 95, 3659–3686, 1990.

Huebert, B. J., Wylie, D. J., Zhuang, L., and Heath, J. A.: Production and loss of methanesulfonate and non-sea salt sulfate in the equatorial Pacific marine boundary layer, Geophys. Res. Lett., 23, 737–740, 1996.

Jayne, J. T., Leard, D. C., Ahang, X., Davidovits, P., Smith, K. A., Kolb, C. E., and Worsnop, D. R.: Development of an aerosol mass spectrometer for size and composition analysis of submicron particles, Aerosol Sci. Tech., 33, 49–70, 2000.

Jimenez, J. L., Jayne, J. T., Shi, Q., Kolb, C. E., Worsnop, D. R., Yourshaw, I., Seinfeld, J. H., Flagan, R. C., Zhang, X., Smith, K. A., Morris, J. W., and Davidovits, P.: Ambient aerosol sampling using the Aerodyne Aerosol Mass Spectrometer, J. Geophys. Res., 108(D7), 8245–8258, 2003.

Kulmala, M., Dal Maso, M., Makela, J. M., Pirjola, L., Vakeva, M., Aalto, P., Miikkulainen, P., Hameri, K., and O'Dowd, C.: On the formation, growth and composition of nucleation mode particles, Tellus, 53B, 479–490, 2001.

Leaitch, W. R., Bottenheim, J. W., Biesenthal, T. A., Li, S.-M., Liu, P. S. K., Asalian, K., Dryfhout-Clark, H., Hopper, F., and Brechtel, F.: A case study of gas-to-particle conversion in an eastern Canadian forest, J. Geophys. Res., 104, 8095–8112, 1999.

Liu, P. S. K., Deng, R., Smith, K. A., Williams, L. R., Jayne, J. T., Canagaratna, M. R., Moore, K., Onasch, T. B., Worsnop, D. R., and Deshler, T.: Transmission efficiency of an aerodynamic focusing lens system: Comparison of model calculations and laboratory measurements for the aerodyne aerosol mass spectrometer, Aerosol Sci. Tech., 41, 721–733, 2007.

Lohmann, U., Broekhuizen, K., Leaitch, R., Shantz, N., and Abbatt, J.: How efficient is cloud droplet formation of organic aerosols?, Geophys. Res. Lett., 31, L05108, 1–4, 2004.

Lohmann, U. and Leck, C.: Importance of submicron surface active organic aerosols for pristine Arctic clouds, Tellus, 57B, 261–268, 2005.

Marshall, J., Lohmann, U., Leaitch, W. R., Shantz, N., Phinney, L., Toom-Sauntry, D., and Sharma, S.: Optical Properties of aerosol particles over the north-east Pacific, J. Appl. Meteorol., 44, 1206–1220, 2005.

National Institute of Standards and Technology (NIST) Standard Reference Database 69: NIST Chemistry WebBook, http://webbook.nist.gov/cgi/cbook.cgi?Name=methanesulfonic+acid&Units=SI&cMS=on, last access: 16 September 2008.

Norman, A.-L., Anlauf, K., Hayden, K., Thompson, B., Brook, J. R., Li, S.-M., and Bottenheim, J.: Aerosol sulphate and its oxidation on the Pacific NW coast: S and O isotopes in $PM_{2.5}$, Atmos. Environ., 40, 15, 2676–2689, 2006.

O'Dowd, C. D., Jimenez, J. L., Bahreini, R., Flagan, R. C., Seinfeld, J. H., Hamerl, K., Pirjola, L., Kulmala, M., Jennings, S. G., and Hoffmann, T.: Marine aerosol formation from biogenic iodine emissions, Nature, 417, 632–636, 2002.

O'Dowd, C. D., Facchini, M. C., Cavalli, F., Ceburnis, D., Mircea, M., Decesari, S., Fuzzi, S., Yoon, Y. J., and Putaud, J.-P.: Biogenically driven organic contribution to marine aerosol, Nature, 431, 676–680, 2004.

Peng, Y., Lohmann, U., Leaitch, R., Banic, C., and Couture, M.: The cloud-albedo droplet effective radius relationship for clean and polluted clouds from RACE and FIRE.ACE, J. Geophys. Res., 107, 4106, AAC 1-1–AAC 1-6, 2002.

Phinney, L., Leaitch, W. R., Lohmann, U., Boudries, H., Worsnop, D. R., Jayne, J. T., Toom-Sauntry, D., Wadleigh, M., Sharma, S., and Shantz, N.: Characterization of Aerosol over the sub-arctic NE Pacific During SERIES, Deep-Sea Res. 2, 53, 2410–2433, 2006.

Pirjola, L., O'Dowd, C. D., Brooks, I. M., and Kulmala, M.: Can new particle formation occur in the clean marine boundary layer?, J. Geophys. Res., 105, 26531–26546, 2000.

Quinn, P. K. and Bates, T.: Regional aerosol properties: Comparisons of boundary layer measurements from ACE 1, ACE 2, Aerosols99, INDOEX, ACE Asia, TARFOX, and NEAQS, J. Geophys. Res., 110, D14202, doi:10.1029/2004JD004755, 2005.

Quinn, P. K., Asher, W. E., and Charleson, R. J.: Equilibria of the marine multiphase ammonia system, J. Atmos. Chem., 14, 11–30, 1992.

Quinn, P. K., Covert, D. S., Bates, T. S., Kaspustin, V. N., Ramsey-Bell, D. C., and McInnes, L. M.: Dimethylsulfide/cloud condensation nuclei/climate system: Relevant size-resolved measurements of the chemical and physical properties of atmospheric aerosol particles, J. Geophys. Res., 98, 10411–10427, 1993.

Russell, L. M., Seinfeld, J. H., Flagan, R. C., Ferek, R. J., Hegg, D. A., Hobbs, P. V., Wobrock, W., Flossmann, A., O'Dowd, C. D., Nielsen, K. E., and Durkee, P. A.: Aerosol dynamics in ship tracks, J. Geophys. Res., 104, 31077–31095, 1999.

Russell, L. M., Noone, K. J., Ferek, R. J., Pockalny, R. A., Flagan, R. C., and Seinfeld, J. H.: Combustion organic aerosol as cloud condensation nuclei in ship tracks, J. Atmos. Sci., 57, 2591–2606, 2000.

Shantz, N. C., Leaitch, W. R., Phinney, L., Mozurkewich, M., and Toom-Sauntry, D.: The effect of organic compounds on the growth rate of cloud droplets in marine and forest settings, Atmos. Chem. Phys., 8, 5869–5887, 2008, http://www.atmos-chem-phys.net/8/5869/2008/.

Shaw, G.: Bio-controlled thermostasis involving the sulfur cycle, Climatic Change, 5, 297–303, 1983.

Sievering, H., Cainey, J., Harvey, M., McGregor, J., Nichol, S., and Quinn, P.: Aerosol non-sea-salt sulphate in the remote marine boundary layer under clear-sky and normal cloudiness conditions: Ocean-derived biogenic alkalinity enhances sea-salt sulfate production by ozone oxidation, J. Geophys. Res., 109, D19317, doi:10.1029/2003JD004315, 2004.

TSI Model 3025A Ultrafine Condensation Particle Counter Instruction Manual, Revision 1, www.tsi.com, July 2002.

Twomey, S.: Pollution and the planetary Albedo, Atmos. Environ., 8, 1251–1256, 1974.

Wang, J., Lee, Y.-N., Daum, P. H., Jayne, J., and Alexander, M. L.: Effects of aerosol organics on cloud condensation nucleus (CCN) concentration and first indirect aerosol effect, Atmos. Chem. Phys., 8, 6325–6339, 2008, http://www.atmos-chem-phys.net/8/6325/2008/.

Weber, R. J., McMurry, P. H., Mauldin, L., Tanner, D. J., Eisele, F. L., Brechtel, F. J., Kreidenweis, S. M., Kok, G. L., Schillawski, R. D., and Baumgardner, D.: A study of new particle formation and growth involving biogenic and trace gas species measured during ACE 1, J. Geophys. Res., 103, 16 385–16 396, 1998.

Yvon, S. A., Saltzman, E. S., Cooper, D. J., Bates, T. S., and Thompson, A. M.: Atmospheric sulfur cycling in the tropical Pacific marine boundary layer (12° S, 135° W): A comparison of field data and model results, 1, Dimethylsulfide, J. Geophys. Res., 101, 6899–6910, 1996.

Zhang, X., Smith, K. A., Worsnop, D. R., Jimenez, J., Jayne, J. T., and Kolb, C. E.: A numerical characterization of particle beam collimation by an aerodynamic lens-nozzle system. Part 1, An individual lens or nozzle, Aerosol Sci. Tech., 36, 631, 2002.

Zorn, S. R., Drewnick, F., Schott, M., Hoffmann, T., and Borrmann, S.: Characterization of the South Atlantic marine boundary layer aerosol using an aerodyne aerosol mass spectrometer, Atmos. Chem. Phys., 8, 4711–4728, 2008, http://www.atmos-chem-phys.net/8/4711/2008/.

Table 1. Properties of the aerosol distribution for points when [MSA] $<0.45\,\mu g\,m^{-3}$ (low MSA; $N=717$) and when [MSA] $>0.45\,\mu g\,m^{-3}$ (high MSA; $N=174$). Percent difference is given for times of "high MSA" relative to "low MSA". D_{eff} refers to the effective physical diameter of the particle distribution.

	SO_4-$CCN_{0.19\%}$	Particle number concentration (cm^{-3})				CCN (V)		mass ($\mu g\,m^{-3}$)		D_{eff} (μm)
	slope	total	$D<58$ nm	$D>58$ nm	$D>86$ nm	0.34%	0.19%	total	$D>58$ nm	
low MSA	0.44	450	275	175	128	0.62	1.5	0.88	0.87	0.22
high MSA	0.64	350	141	209	152	0.80	2.0	1.1	1.1	0.22
% diff	**45%**	−22%	−49%	**19%**	**19%**	**29%**	**30%**	**26%**	**27%**	**0%**

Table A1. Solution mixtures and size distribution characteristics of MSA identification trials using the Q-AMS. AmmSul refers to Ammonium Sulphate, MSA to Methansulphonic Acid.

Trial	Run #	Composition	Number Concentration (cm^{-3})	Physical Diameter (nm)	Plot
1	2409	AmmSul	5400	300	A1
2	4401	MSA+AmmSul	500	300	A2
3	4396	MSA	2000	300	A3, A5
4	4403	n/a	0	n/a	A4

Table A2. Fragmentation table resulting from controlled laboratory trials running atomized Ammonium Sulphate and MSA through the Q-AMS. MSA fragments are based on the fragments at *m/z* 79 and 96. Fragments whose formulas have been modified from the previous version of the fragmentation table (Allan et al., 2004) are noted in boldface.

m/z	frag_MSA	frag_sulphate	frag_organic
1			
2			
3			
4			
5			
6			
7			
8			
9			
10			
11			
12			12
13			13
14			
15	**2.16*frag_msa[79],2.16*frag_msa[96]**		**15,-frag_NH4[15],-frag_air[15],-frag_msa[15]**
16		frag_SO3[16]	0.04*frag_organic[18]
17		frag_SO3[17]	0.25*frag_organic[18]
18		frag_SO3[18]	1*frag_organic[44]
19		frag_SO3[19]	0.000691*frag_organic[18],0.002*frag_organic[17]
20		frag_SO3[20]	0.002*frag_organic[18]
21			
22			
23			
24		frag_SO3[24],frag_H2SO4[24]	24,-frag_sulphate[24]
25			25
26			26
27			27
28			
29	**0.22*frag_msa[79],0.22*frag_msa[96]**		**29,-frag_air[29],-frag_msa[29]**
30			0.022*frag_organic[29]
31	**0.51*frag_msa[79],0.51*frag_msa[96]**		
32		frag_SO3[32],frag_H2SO4[32]	
33		frag_SO3[33],frag_H2SO4[33]	
34		frag_SO3[34],frag_H2SO4[34]	
35			
36			
37			37,-frag_chloride[37]
38			38,-frag_chloride[38],-frag_air[38]

Table A2. Continued.

m/z	frag_MSA	frag_sulphate	frag_organic
39			
40			
41			41,-frag_K[41]
42			42
43			43
44			44,-frag_air[44]
45	**0.23*frag_msa[79],0.23*frag_msa[96]**		**45,-frag_msa[45]**
46			
47			
48		frag_SO3[48],frag_H2SO4[48]	0.5*frag_organic[62]
49		frag_SO3[49],frag_H2SO4[49]	49,-frag_sulphate[49]
50		frag_SO3[50],frag_H2SO4[50]	50,-frag_sulphate[50]
51			51
52		frag_SO3[52],frag_H2SO4[52]	52,-frag_sulphate[52]
53			53
54			54
55			55
56			56
57			57
58			58
59			59
60			60
61			61
62			62
63			63,-frag_nitrate[63]
64		frag_SO3[64],frag_H2SO4[64]	**frag_organic[50]**
65	**0.37*frag_msa[79],0.37*frag_msa[96],-frag_sulphate[65]**	frag_SO3[65],frag_H2SO4[65]	**frag_organic[51]**
66		frag_SO3[66],frag_H2SO4[66]	66,-frag_sulphate[66]
67			67
68			68
69			69
70			70
71			71
72			72
73			73
74			74
75			75
76			76
77			77
78	**0.24*frag_msa[79],0.24*frag_msa[96]**		**78,-frag_msa[78]**
79	**79,-frag_organic[79]**		**frag_organic[93]**
80		frag_SO3[80],frag_H2SO4[80]	0.75*frag_organic[94]
81		frag_H2SO4[81]	0.5*frag_organic[67],0.5*frag_organic[95]
82		frag_SO3[82],frag_H2SO4[82]	82,-frag_sulphate[82]
83		frag_H2SO4[83]	83,-frag_sulphate[83]
84		frag_SO3[84],frag_H2SO4[84]	84,-frag_sulphate[84]
85		frag_H2SO4[85]	85,-frag_sulphate[85]

Table A2. Continued.

m/z	frag_MSA	frag_sulphate	frag_organic
86			86
87			87
88			88
89			89
90			90
91			91
92			92
93			93
94			94
95			95
96	**96,-frag_organic[96]**		**0.5*frag_organic[110],0.5*frag_organic[82]**
97			97
98		frag_H2SO4[98]	0.5*frag_organic[84],0.5*frag_organic[112]
99		frag_H2SO4[99]	99,-frag_sulphate[99]
100		frag_H2SO4[100]	100,-frag_sulphate[100]
101			101
102		frag_H2SO4[102]	102,-frag_sulphate[102]

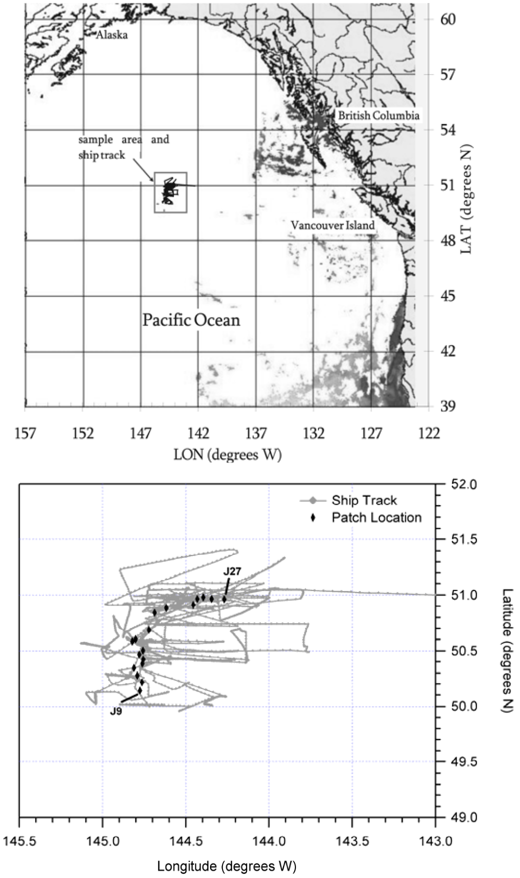

Fig. 1. (a) Map of sample area and ship track. Measurements were taken near Station Papa, in the Sub-Arctic North East Pacific Ocean, 142°–155° W, 48°–51° N. **(b)** Expanded view of El Puma ship track, and patch location as it drifted towards the northeast, from 9 July to 27 July 2002.

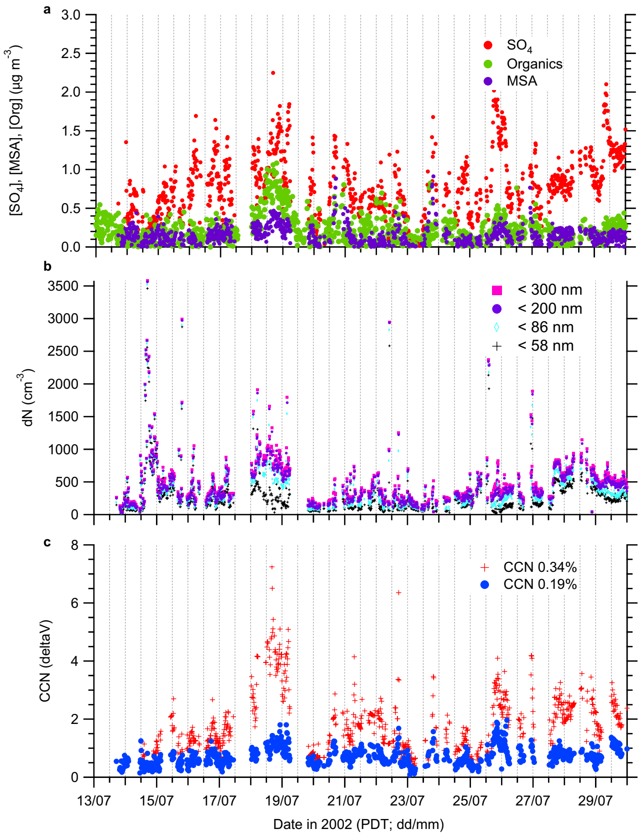

Fig. 2. Time series of data collected 13–30 July 2002, in the Northeast Pacific Ocean. The graphs show **(a)** mass concentrations of sulphate, MSA, and organics measured by the Q-AMS, **(b)** number concentration of particles in four size intervals measured by the SMPS, and **(c)** deltaV (approximately proportional to number concentration) for CCN active at 0.19 and 0.34% supersaturation.

Title Page
Abstract | Introduction
Conclusions | References
Tables | Figures
◀| |▶
◀ ▶
Back | Close
Full Screen / Esc
Printer-friendly Version
Interactive Discussion

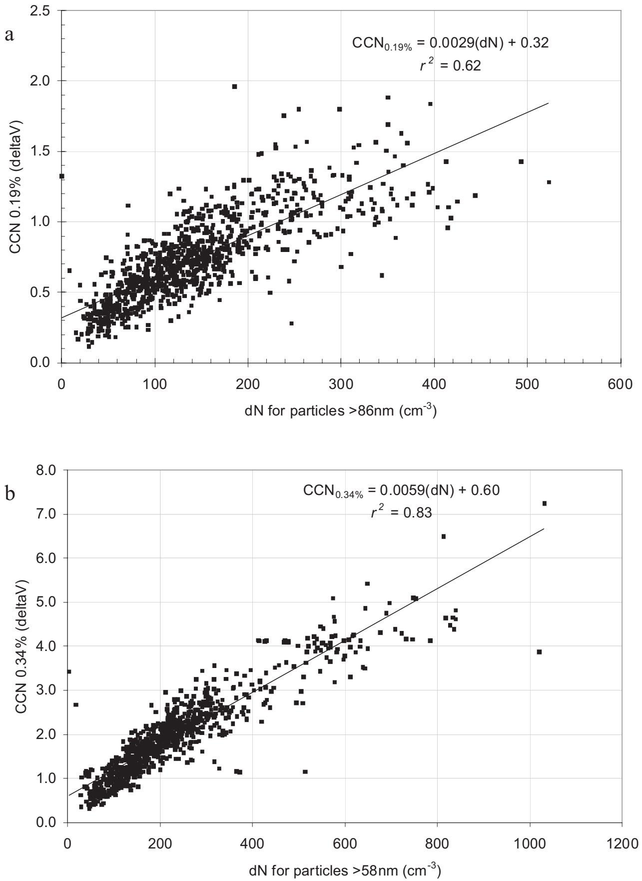

Fig. 3. Correlation of CCN deltaV measured in the NE Pacific, 13–30 July 2002, with number concentrations of particles having diameters greater than the theoretical critical diameters of **(a)** 86 nm and **(b)** 58 nm for CCN active at 0.19% (CCN$_{0.19\%}$) and 0.34% (CCN$_{0.34\%}$), respectively. Linear trendlines and correlation coefficients (r^2) are shown.

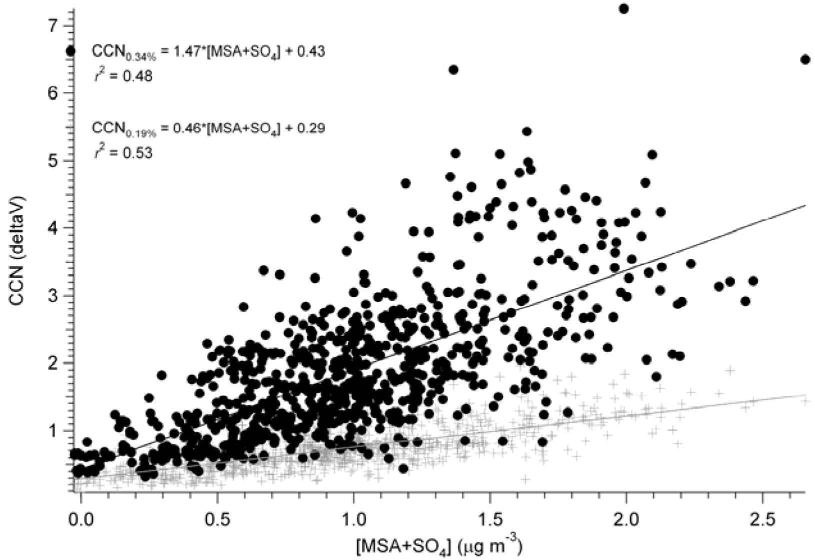

Fig. 4. Correlations of $CCN_{0.19\%}$ and $CCN_{0.34\%}$ each with [MSA+SO_4] for 13–30 July 2002. Linear trendlines and correlation coefficients (r^2) are shown.

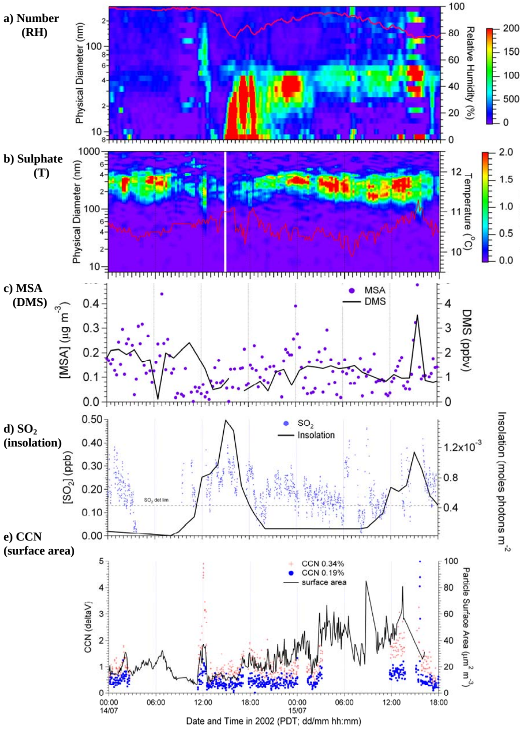

Fig. 5. Image plots of **(a)** dN/d log D and **(b)** sulphate dM/d log D (colour bars) vs. time (x-axis) and physical diameter (left y-axis); relative humidity is overlaid as a line on plot **(a)**, and temperature on **(b)**, corresponding to the right y-axes. Time series of **(c)** MSA (left y-axis) and DMS (right y-axis) concentrations, **(d)** SO_2 concentration (left y-axis) and insolation (right y-axis) and **(e)** CCN active at two supersaturations (left y-axis) and surface area (right y-axis). All plots are for the time period 14 July 00:00–15 July 18:00. Note that the left y-axis is scaled differently in (a) than in (b). AMS aerodynamic diameters were converted to physical diameters using a density of 1.8 g cm^{-3}.

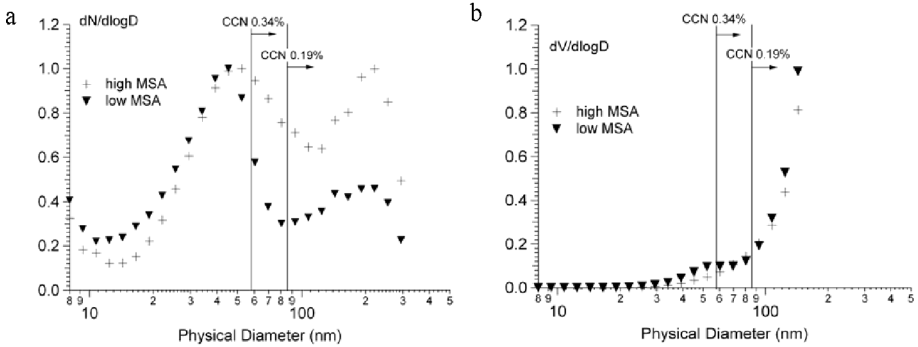

Fig. 6. **(a)** Normalized size distribution of particle number concentration for times when peak MSA concentrations are greater than 0.45 µg m^{-3} (high MSA), and less than 0.45 µg m^{-3} (low MSA). **(b)** Mass concentration derived from the number concentration for the conditions described in (a). Vertical bars indicate the activation diameter at each supersaturation. The number distributions show more particles with diameters larger than the CCN activation diameter for the high-MSA case, whereas the volume distribution shows little change.

Title Page
Abstract
Introduction
Conclusions
References
Tables
Figures
◀◀
▶▶
◀
▶
Back
Close
Full Screen / Esc
Printer-friendly Version
Interactive Discussion

Title Page
Abstract | Introduction
Conclusions | References
Tables | Figures
|◀ | ▶|
◀ | ▶
Back | Close
Full Screen / Esc
Printer-friendly Version
Interactive Discussion

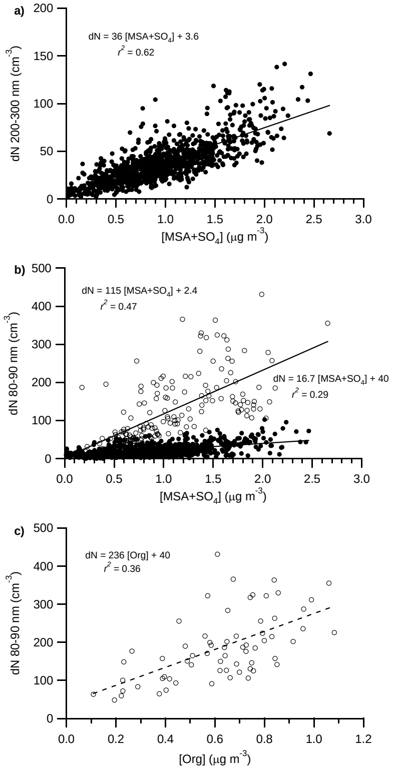

Fig. 7. **(a)** Correlation of [MSA+SO$_4$] with the concentrations of particles with physical diameters between 200 and 300 nm, for 13–30 July 2002; **(b)** correlation of [MSA+SO$_4$] with concentrations of particles with physical diameters between 80 and 90 nm. The data are divided into two trends, the upper trend identified by high particle number concentration; **(c)** correlation of organics with the concentration of particles with physical diameters between 80 and 90 nm, for the points located in the upper trend in Fig. 6a. The best-fit linear trendlines and correlation coefficients are shown.

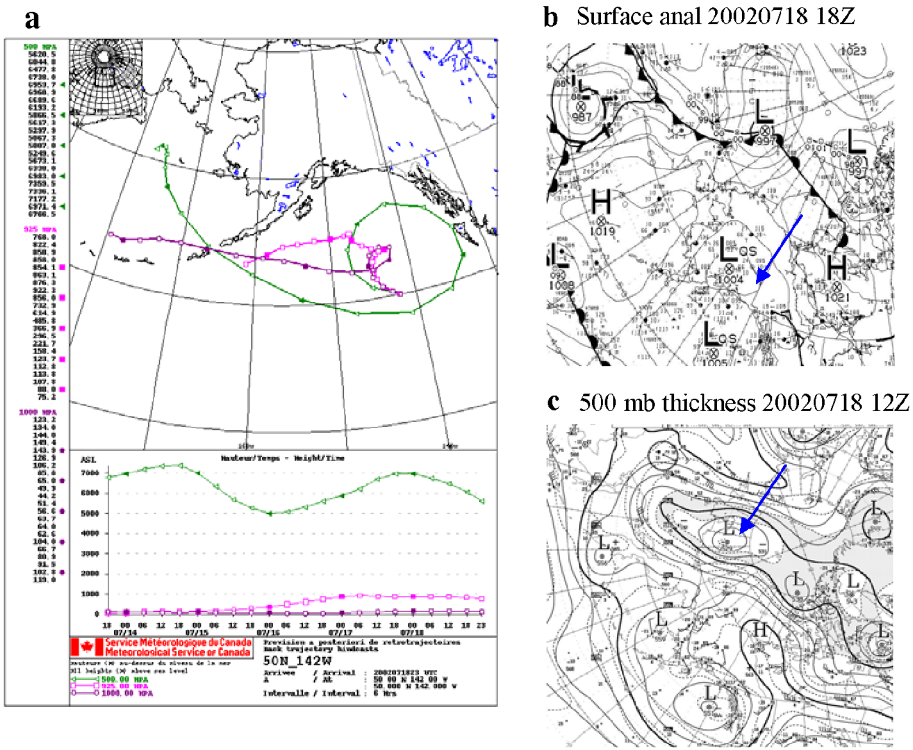

Fig. 8. **(a)** Five-day Canadian Meteorological Centre back trajectory for the sample location, 50° N 142° W, near Station Papa, ending 18 July 23:00. The purple curve indicates the 1000 mb (surface) trajectory; the pink curve represents the 925 mb (long-range-transport) trajectory, and the green curve indicates the 500 mb trajectory (steering flow). The lower graph shows the altitude (in m above sea level) of the air parcels along their respective trajectories. Surface **(b)** and upper air **(c)** analyses verify a stagnant system circling in the sample region on 18 July. The location of the quasi-stationary low is marked with a blue arrow.

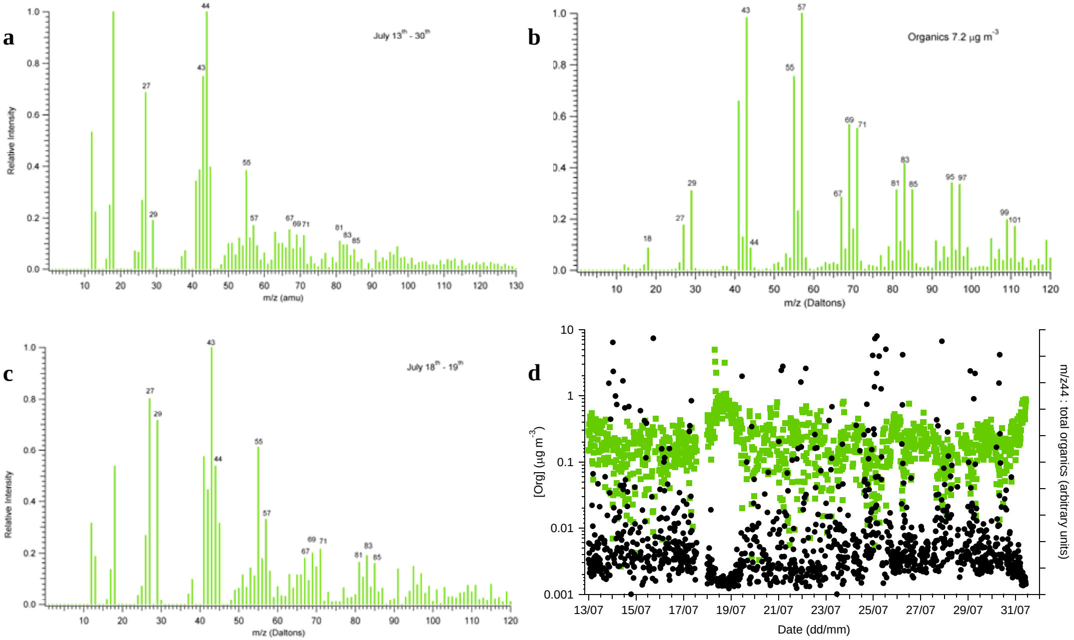

Fig. 9. Mass spectra of organics, plotted as relative intensity, **(a)** for the entire sample period, excluding ship plumes and the 18 July case, **(b)** during direct fumigation by ship exhaust (Phinney et al., 2006), and **(c)** for the period of high organics mass concentration, 18 July. Plot **(d)** shows the total mass concentration of organics (left *y*-axis; log scale) and the ratio of the voltage intensity of the signal at *m/z* 44 to total organic mass for 18 July ("*m/z* 44: total"; right *y*-axis), after periods of direct fumigation are removed. The ratio depicts the relative amount of oxygenated organics in the air; on 18 July a reduction in the ratio and in the scatter of the values is evident indicating a relatively less oxygenated organic and a distinct source.

Title Page
Abstract
Introduction
Conclusions
References
Tables
Figures
◀
▶
Back
Close
Full Screen / Esc
Printer-friendly Version
Interactive Discussion

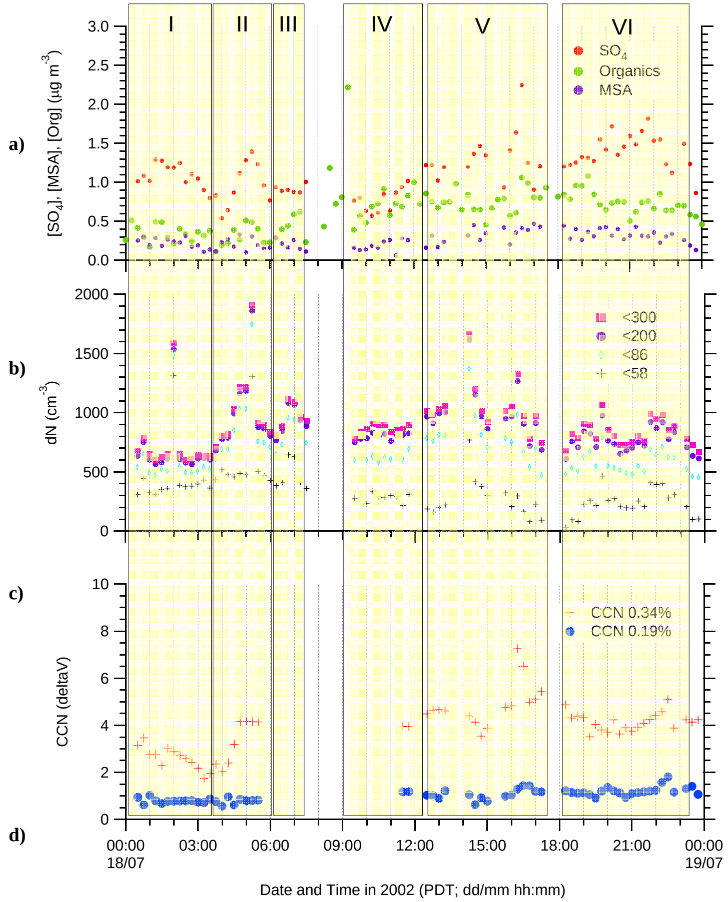

Fig. 10. Expanded view of Fig. 2, centred on the increase in organics mass concentration and number concentration 18 July. The plot is divided into six time intervals: Period 1 00:00–03:45, Period II 03:45–06:00, Period III 06:00–07:30, Period IV 09:00–12:30, Period V: 12:30–17:30, and Period VI: 18:00–23:30.

Title Page
Abstract
Introduction
Conclusions
References
Tables
Figures
◀◀
▶▶
◀
▶
Back
Close
Full Screen / Esc
Printer-friendly Version
Interactive Discussion

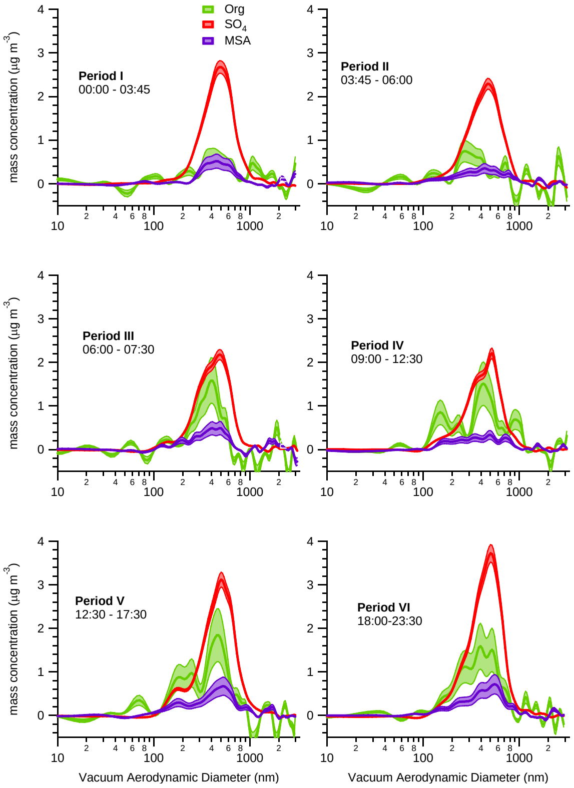

Fig. 11. Evolution of the mass distributions of organics, sulphate, and MSA measured by the Q-AMS 18 July, during Period I 00:00–03:45, Period II 03:45–06:00, Period III 06:00–07:30, Period IV 09:00–12:30, Period V 12:30–17:30, and Period VI 18:00–23:30, plotted against vacuum aerodynamic diameter, D_{va}. The thickness of the Q-AMS curves indicates the uncertainty range.

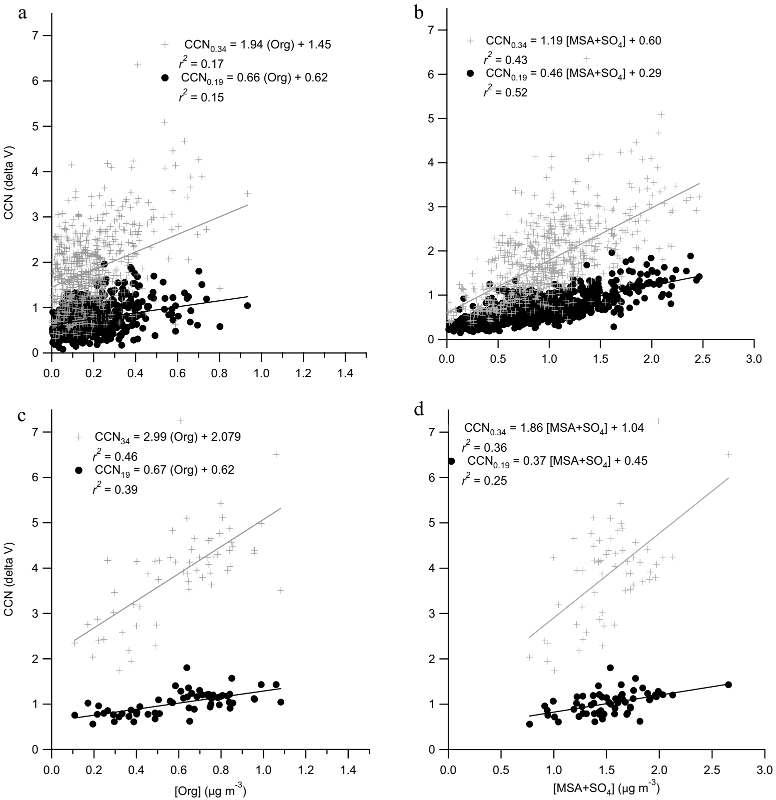

Fig. 12. Correlations of CCN with mass concentrations of organics and sulphur species: **(a)** and **(b)** show the correlation of CCN with organics and with [MSA+SO$_4$], respectively, for the entire sample period excluding 18 July; **(c)** and **(d)** show the correlations for points on 18 July only. The better correlation in (b) compared with (a) indicates that, in general, the MSA and sulphate control the CCN. However, the improved correlations in (c) compared with (a) indicate that for 18 July the organics control the CCN, consistent with the results shown in Figs. 10 and 11.

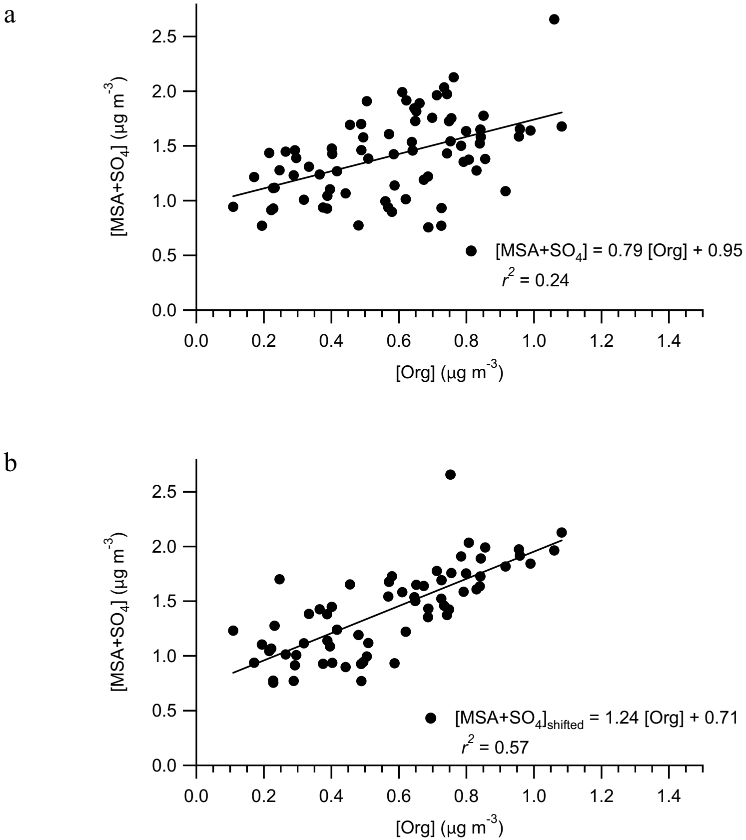

Fig. 13. Correlation of [MSA+SO$_4$] with organics for 18 July. In **(a)** the series are plotted directly against each other, and show only a weak correlation. In **(b)** the [MSA+SO$_4$] series is first shifted back in time and then plotted against organics. The best correlation was seen for a time-shift of 2.5 h (shown here), suggesting that on 18 July the MSA and sulphate condensed onto the organics over a time scale of several hours.

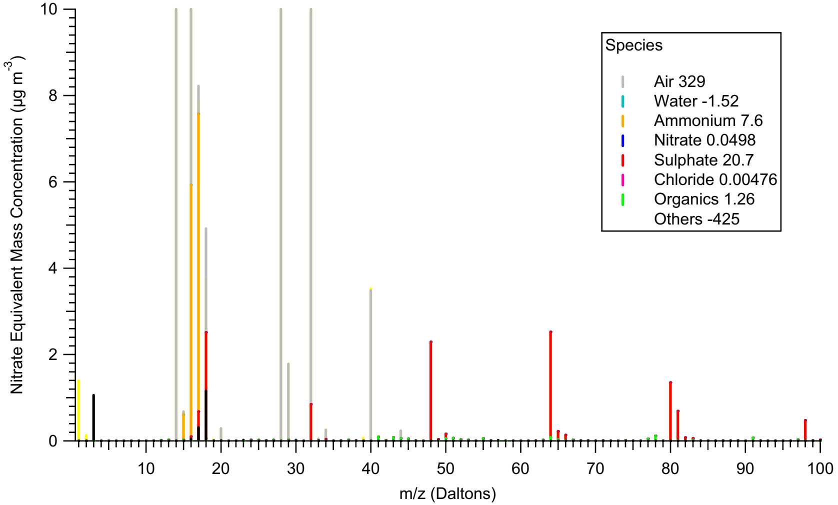

Fig. A1. Q-AMS mass spectrum for trial 1, $(NH_4)_2SO_4$ 5400 particles cm^{-3} at 300 nm physical diameter.

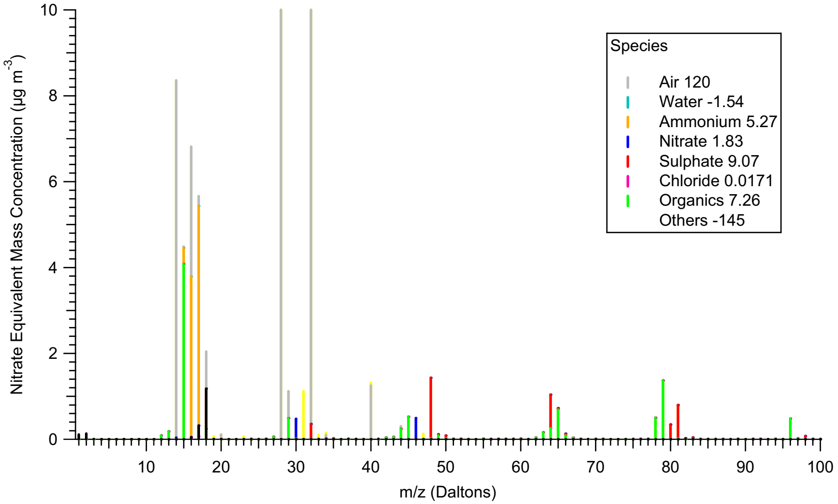

Fig. A2. Q-AMS mass spectrum for trial 2, MSA+$(NH_4)_2SO_4$ 500 particles cm^{-3} at 300 nm physical diameter, processed with the previous version of the fragmentation table (which does not analyse for MSA).

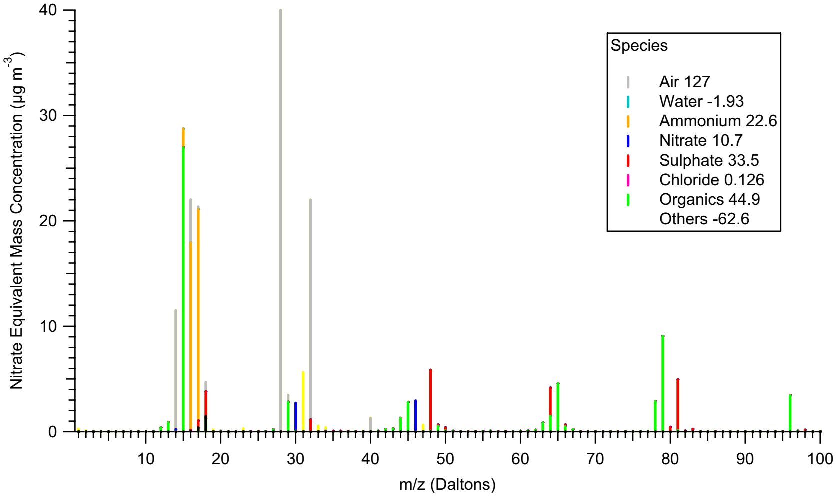

Fig. A3. Q-AMS mass spectrum for trial 3, MSA 2000 particles cm^{-3} at 300 nm physical diameter, processed with the previous version of the fragmentation table (which does not analyse for MSA).

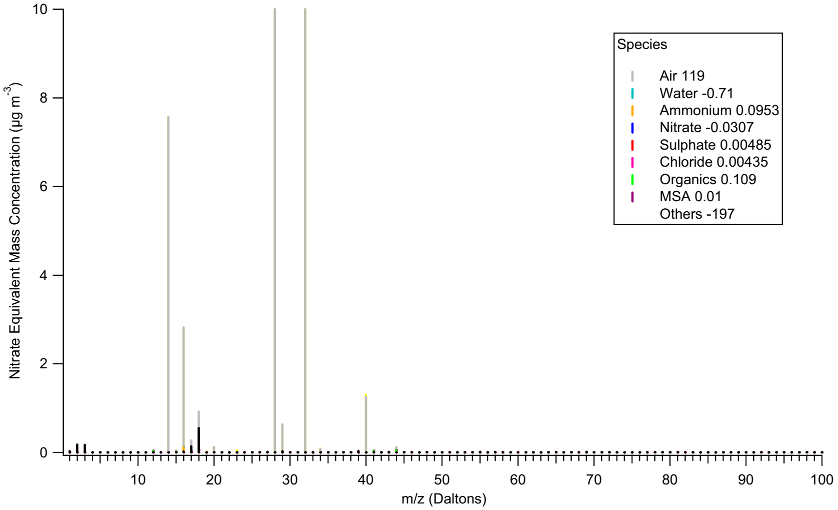

Fig. A4. Q-AMS mass spectrum for trial 4, 0 particles cm^{-3}.

Title Page
Abstract | Introduction
Conclusions | References
Tables | Figures
◀▌ | ▌▶
◀ | ▶
Back | Close
Full Screen / Esc
Printer-friendly Version
Interactive Discussion

Title Page
Abstract
Introduction
Conclusions
References
Tables
Figures
◀▌ ▶▌
◀ ▶
Back
Close
Full Screen / Esc
Printer-friendly Version
Interactive Discussion

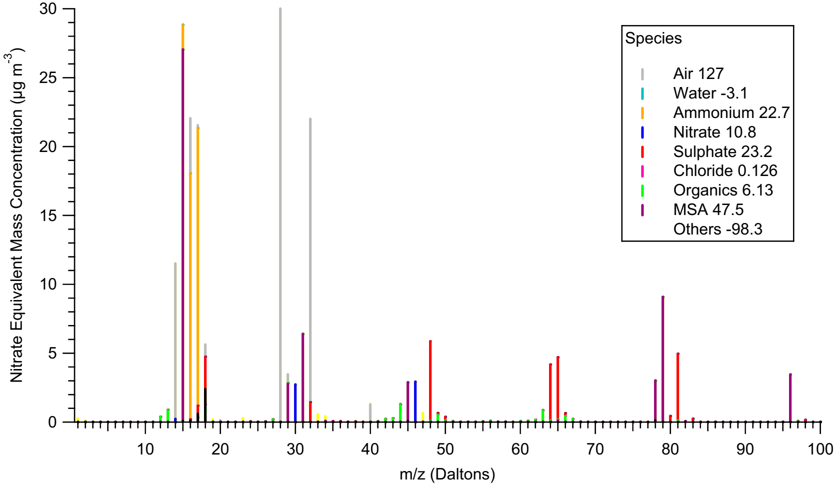

Fig. A5. Q-AMS mass spectrum for trial 3, MSA 2000 particles cm^{-3} at 300 nm physical diameter, processed with the new fragmentation table which includes MSA. Note that organics and sulphate masses have decreased compared with Fig. A3, due to the MSA fragments that were previously attributed to sulphate and organics now identified as MSA. Some sulphate fragments (e.g. *m/z* 65 and *m/z* 98) remain due to small errors in the fragmentation table at the time of analysis, and result in an underestimation of MSA of approximately 25%.